Joint Chromatic Aberration correction and Demosaicking

Mritunjay Singh and Tripurari Singh

Image Algorithmics, 521 5th Ave W, #1003, Seattle, WA, USA 98119

ABSTRACT

Chromatic Aberration of lenses is becoming increasingly visible with the rise of sensor resolution, and methods to algorithmically correct it are becoming increasingly common in commercial systems. A popular class of algorithms undo the geometric distortions after demosaicking. Since most demosaickers require high frequency correlation of primary colors to work effectively, the result is artifact-ridden as Chromatic Aberration destroys this correlation.

The other existing approach of undistorting primary color images before demosaicking requires resampling of sub-sampled primary color images and is prone to aliasing. Furthermore, this algorithm cannot be applied to panchromatic CFAs.

We propose a joint demosaicking and Chromatic Aberration correction algorithm that is applicable to both panchromatic and primary color CFAs and suffers from none of the above problems. Our algorithm treats the mosaicing process as a linear transform that is invertible if luminance and chrominance are appropriately bandlimited. We develop and incorporate Chromatic Aberration corrections to this model of the mosaicing process without altering its linearity or invertibility. This correction works for both space variant linear filter demosaicking and the more aggressive compressive sensing reconstruction.

Keywords: Chromatic Aberration, Demosaicking, Color, Filter, Linear

1. INTRODUCTION

Wavelength dependent refractive properties of camera optics can lead to geometric misalignment of the image in different colors, known as *lateral chromatic aberration*, and misfocusing of different colors, known as *longitudinal chromatic aberration*. Since Sensor technology is rapidly outpacing lens technology, previously neglected lens flaws, such as Chromatic Aberration (CA), are becoming increasingly objectionable. This problem is especially acute in mass market cameras where inexpensive low performance lenses are mated with high resolution sensors.

Algorithmic correction of CA was first addressed by[1] , and refined by[2] ,[3] ,[4] . One color plane was defined as the reference and the other two were "warped" by resampling on lattice distorted according to the lateral CA present. Blue was chosen as the reference color plane by[1] , but[2] ,[3] ,[4] picked green owing to its higher SNR and less warping from the non-reference color planes.

Lateral CA was modeled by a radially symmetric polynomial function,[1],[2],[3].[4] Mallon and Whelon[3] , in particular, used a sophisticated lens model that allowed them to predict lateral CA with high accuracy. Model parameters were determined using special target images, such as checker boards, with plenty of "interest points" such as edges and corners[1] ,[2] ,[4] . Interest points in the different color planes were matched using cubic splines[1] , least squares[2] ,[3] or Difference of Gaussians[4] .

In addition to lateral CA,[4] addressed longitudinal CA and in camera sharpening. In contrast to the above techniques Chung et al.[5] dispensed with image warping altogether electing, instead, to identify and desaturate edges with color fringes. No training with target images is required in their system. Instead they identify and learn the characteristics of edges free from color fringes in the image to be corrected and use this information to identify the fringed edges. Both lateral and longitudinal CA are ameliorated by their method.

Commercially, lateral CA correction has been incorporated in-camera by Nikon and in image processing software from Adobe, DxO Labs and Phase One and in the open source PTLens and the raw converter dcraw.

Further author information: {msingh, tsingh}@imagealgorithmics.com (send correspondence to M.S.)

Patent pending

Most raw converters offer both lens models for automatic correction as well as manual tools that allow the user to alter the magnification of red and blue color planes so as to better align with green.

Most academic solutions and post processing software apply CA correction after the sensor data has been demosaicked. Since most demosaickers require high frequency correlation of primary colors to work effectively, the result is artifact-ridden as CA destroys this correlation.

Most raw conversion software, on the other hand, apply CA correction on red and blue channels before demosaicking. This is also problematic as each color by itself is sub-sampled and may be aliased. Furthermore, pre-demosaic CA cannot be applied to panchromatic CFAs. When applied to the Bayer CFA, however, pre-demosaic CA correction results in better sharpness and less artifacting than post-demsoaic CA correction, and thus represents the current state of the art.

We propose a joint demosaicking and CA correction algorithm that suffers from none of the above problems. This algorithm generalizes the demosaicker of[6] to include CA correction without significantly altering its underlying assumptions or incurring performance penalties. Furthermore, this algorithm is applicable to both panchromatic and primary color CFAs.

2. CHROMATIC ABERRATION AS A LINEAR OPERATION

In this paper we adopt the image warping view of lateral CA, and aim to rectify the problem by geometrically aligning color planes instead of desaturating color-fringed edges. We do not address the problem of measuring and modeling lateral CA and direct the reader to papers cited in the introduction for approaches to this problem.

Consider a discrete image, or an image patch, with (N_1, N_2) pixels. Denote the R, G, B color planes of the aberrated image by $x'_i(\boldsymbol{n})$, and those of the aberration free image by $x_i(\boldsymbol{n}), i \in \{r, g, b\}, \boldsymbol{n} = (n_1, n_2), 1 \leq n_1 \leq N_1, 1 \leq n_2 \leq N_2$. Given the geometric distortion due to lateral CA, the aberrated image can be obtained from its aberration free version by resampling it on a suitably distorted lattice, as long as the Nyquist limit is not violated in the process. Since resampling is a linear operation, and violation of the Nyquist limit is of no practical concern given that lateral CA is limited to a fraction of a percentage, lateral CA can be modeled by a space variant linear operator $h_i^{lat}(\boldsymbol{n}), i \in \{r, g, b\}$. For a detailed derivation of $h_i^{lat}(\boldsymbol{n}), i \in \{r, g, b\}$, see appendix A.

We also address longitudinal CA by modeling it as a space variant sharpening/blurring operation, represented by the space variant linear operator $h^{long}(\boldsymbol{n})_i, i \in \{r, g, b\}$, so that the combined CA is,

$$h_i(\boldsymbol{n}) = h_i^{lat}(\boldsymbol{n}) * h_i^{long}(\boldsymbol{n}), i \in \{r, g, b\} \tag{1}$$

3. JOINT DEMOSAICKING AND CHROMATIC ABERRATION CORRECTION

A photosite located at $\boldsymbol{n} = (n_1, n_2), 1 \leq n_1 \leq N_1, 1 \leq n_2 \leq N_2$ filters the incident light of the aberrated image $\boldsymbol{x}'(\boldsymbol{n}) = \begin{bmatrix} x'_r(\boldsymbol{n}) & x'_g(\boldsymbol{n}) & x'_b(\boldsymbol{n}) \end{bmatrix}^T$ through color filter array $\boldsymbol{c}(\boldsymbol{n}) = \begin{bmatrix} c_r(\boldsymbol{n}) & c_g(\boldsymbol{n}) & c_b(\boldsymbol{n}) \end{bmatrix}$ and measures the resulting noise-free, scalar signal $y(\boldsymbol{n})$, where

$$y(\boldsymbol{n}) = \boldsymbol{c}(\boldsymbol{n}) \cdot \boldsymbol{x}'(\boldsymbol{n}) \tag{2}$$

Let the row-major column vector versions of y and the color planes of $\boldsymbol{x}'$, $\boldsymbol{c}$ be $\tilde{\boldsymbol{y}}, \tilde{\boldsymbol{x}}'_i, \hat{\boldsymbol{c}}_i, i \in \{r, g, b\}$. Define $\tilde{\boldsymbol{c}}_i, i \in \{r, g, b\}$ as a diagonal matrix such that $\tilde{\boldsymbol{c}}_i(n, n) = \hat{\boldsymbol{c}}_i(n)$. Let $\tilde{\boldsymbol{x}}' \equiv \begin{bmatrix} \tilde{\boldsymbol{x}}'_r & \tilde{\boldsymbol{x}}'_g & \tilde{\boldsymbol{x}}'_b \end{bmatrix}^T$ be a column vector formed by concatenating $\tilde{\boldsymbol{x}}'_i, i \in \{r, g, b\}$ and $\tilde{\boldsymbol{c}} = \begin{bmatrix} \tilde{\boldsymbol{c}}_r & \tilde{\boldsymbol{c}}_g & \tilde{\boldsymbol{c}}_b \end{bmatrix}$ be a matrix formed by concatenating $\tilde{\boldsymbol{c}}_i, i \in \{r, g, b\}$. Equation 2 can now be re-written as,

$$\tilde{\boldsymbol{y}} = \tilde{\boldsymbol{c}} \cdot \tilde{\boldsymbol{x}}' \tag{3}$$

Let $\boldsymbol{x}(\boldsymbol{n}) = \begin{bmatrix} x_r(\boldsymbol{n}) & x_g(\boldsymbol{n}) & x_b(\boldsymbol{n}) \end{bmatrix}^T$ be the aberration free image and let $\tilde{\boldsymbol{x}}_i$ be the row major column vector versions of $x_i, i \in \{r, g, b\}$. Let $\tilde{\boldsymbol{x}} = \begin{bmatrix} \tilde{\boldsymbol{x}}_r & \tilde{\boldsymbol{x}}_g & \tilde{\boldsymbol{x}}_b \end{bmatrix}^T$ be the column vector formed by concatenating $\tilde{\boldsymbol{x}}_i, i \in \{r, g, b\}$. Cast the CA operator $h_i(\boldsymbol{n}), \forall i \in \{r, g, b\}$ as a matrix $\tilde{\boldsymbol{h}}$ so that $\tilde{\boldsymbol{h}} \cdot \tilde{\boldsymbol{x}}$ yields the aberrated image $\tilde{\boldsymbol{x}}'$. Equation 3 can now be re-written as,

$$\tilde{\boldsymbol{y}} = \tilde{\boldsymbol{c}} \cdot \tilde{\boldsymbol{h}} \cdot \tilde{\boldsymbol{x}} \tag{4}$$

This system of linear equations can be solved to determine $\tilde{\boldsymbol{x}}$ if the rank of $\tilde{\boldsymbol{c}} \cdot \tilde{\boldsymbol{h}}$ is no less than $|\tilde{\boldsymbol{x}}|$, where $|.|$ denotes cardinality. However, since the rank of matrix $\tilde{\boldsymbol{c}} \cdot \tilde{\boldsymbol{h}}$ cannot exceed $|\tilde{\boldsymbol{y}}|$ which itself is one third of the cardinality of $\tilde{\boldsymbol{x}}$, for the case of three basic colors, this is not possible without additional constraints. These may include conditions such as signal band-limitedness, low chrominance bandwidth, or sparse spectral support.

Next, consider a N_1, N_2 point 2D DFT matrix D so that $D \cdot \tilde{\boldsymbol{x}}_i, i \in \{r, g, b\}$ determines the DFT of $\tilde{\boldsymbol{x}}_i$. Also consider a color transform matrix K from RGB to a suitably chosen luminance, chrominance color space. Define $G = K \otimes D$, the Kronecker product of K, D. It is easy to see that $G \cdot \tilde{\boldsymbol{x}}$ yields the DFT coefficients of $K \cdot \tilde{\boldsymbol{x}}$, the image in the luminance, chrominance color space.

Next, construct a matrix $\boldsymbol{s}$ consisting of rows of G that represent the DFT coefficients of color components to be set to zero. We augment the system of equations 4 by replacing $\tilde{\boldsymbol{c}} \cdot \tilde{\boldsymbol{h}}$ with $B = \begin{bmatrix} \tilde{\boldsymbol{c}} \cdot \tilde{\boldsymbol{h}} \\ \boldsymbol{s} \end{bmatrix}$ and $\tilde{\boldsymbol{y}}$ with $\boldsymbol{y}' = \begin{bmatrix} \tilde{\boldsymbol{y}} \\ 0_p \end{bmatrix}$, where 0_p is a vector of p zeros and p is the number of rows of $\boldsymbol{s}$ to obtain:

$$\boldsymbol{y}' = B \cdot \tilde{\boldsymbol{x}} \tag{5}$$

This results in the solution for the demosaicked, aberration free image

$$\tilde{\boldsymbol{x}} = B^{-1} \cdot \boldsymbol{y}' \tag{6}$$

where B^{-1} is the pseudo inverse of B.

The algorithm developed above can be implemented as a space variant FIR and can be readily extended to incorporate edge adaptive directional spectral models, such as that of.[6] Doing so requires using two or more image models, each with greater bandwidth in a privileged direction than in any other, setting up and solving equation 5 accordingly and picking the one that works best for each image locality.

4. PRACTICAL CONSIDERATIONS

Section 3 shows that the mosaicking-demosaicking process can be made transparent to any linear distortion correction. To the extent the linear image distortion does not discard image information, and can be reversed on a faithful representation of the optical image, the same can be done with a mosaiced image.

One area of concern, however, is the effective perturbation of the CFA pattern by the image warping process of lateral CA. The change in CFA carriers, and thereby the change in spectral packing of signals in the mosaicked image, is itself tiny and can be neglected. While this has no effect on the reconstruction of noise free images, the noise of noisy images can be slightly uneven by numerical stability problems. In the case of Bayer, for example, lateral CA can result in the red and blue pixels "moving" and overlapping with the green pixels. This leaves "holes" in the mosaiced image where no color is sensed which, in turn, degrades the numerical stability of reconstructing these pixels while improving the numerical stability of reconstructing pixels where more than one color is sensed.

Random CFAs also suffer from uneven numerical stability resulting from "holes" in the mosaiced image where no color is sensed. However, these "holes" are in a random pattern instead of being in a simple regular pattern. This randomizes the resulting noise unevenness and makes them less visible and more amenable to noise reduction.

In addition to the choice of CFA, reconstruction performance depends on the choice of color space as well as the bandwidth of its luminance and chrominance signals. Opponent red-green and yellow-blue color space is especially effective at reducing chrominance energy, and thereby improving reconstruction quality.[7] Joint demosaicking and lateral CA correction is no different than plain demosaicking in this regard.

5. EXPERIMENTAL RESULTS

We empirically tested our joint lateral CA correction and demosaicking algorithm with a Matlab simulation. We used a simple model of CA wherein green served as the reference image and red, blue were magnified by different amounts: blue was enlarged by 0.52% and red was shrunk by the same factor compared to green.

The imaging pipeline simulated consisted of a diffraction limited lens model, a birefringent OLPF, box filtration due to non-zero pixel size, CFA filtration, demosaicking and inverse box filtering. The optical pipeline was simulated with greater than Nyquist resolution in order to capture the aliasing due to high frequency leakage through the OLPF. Reconstructed images were compared, in terms of CPSNR, with the input image put through the same imaging pipeline except for the mosaicing-demosaicking step. S-CIELAB[8] and luminance SSIM[9] were also computed but found to be consistent with CPSNR and not reported. Typical optical parameter values for compact cameras and full frame 35mm DLSRs, shown in Table 1, were used.

Parameter	Compact	DSLR
Lens airy disc diameter	3 pixels	1 pixel
Birefringent OLPF shift	none	1 pixel
Box filtering fill factor	100%	100%
Undersampling factor	1x	1.5x

Table 1. Imaging pipeline simulation parameters.

The proposed demosaicking algorithm was compared to five state of the art demosaickers for the Bayer CFA: DLMMSE,[10] AHD,[11] MHC,[12] POCS[13] and LSLCD.[14] For each of these five demosaickers, chromatic aberration correction was performed both pre-demosaicking and post-demosaicking. The proposed demosaicking algorithm was configured to use the Bayer CFA and compute a space variant FIR filter with 11x11 kernel size. It was tuned to reconstruct luminance at a resolution of 80.1% of the Nyquist limit and chrominance at 52.8% of the luminance resolution, which is competitive with commercial systems. Other demosaicker outputs were post filtered to the same resolutions which made no perceptible difference in the image quality and marginally improved their CPSNRs. Images from both the Kodak set and the newer McMaster[15] set (previously known as the IMAX set) were used. Results are shown in Table 2.

Image set	Pre					Joint	Post				
	DLMMSE	MHC	AHD	POCS	LSLCD	Proposed	DLMMSE	MHC	AHD	POCS	LSLCD
McMaster	42.37	43.35	40.78	40.94	39.33	**47.63**	39.13	40.77	37.84	37.55	35.97
Kodak	47.33	45.77	46.57	46.36	44.68	**54.20**	39.31	40.71	38.40	37.87	36.70

Image set	Pre					Joint	Post				
	DLMMSE	MHC	AHD	POCS	LSLCD	Proposed	DLMMSE	MHC	AHD	POCS	LSLCD
McMaster	37.61	38.17	36.55	36.19	35.15	**41.50**	35.61	36.78	34.62	34.12	33.06
Kodak	41.23	40.06	40.94	40.16	39.31	**45.85**	36.64	37.36	36.02	35.44	34.66

Table 2. CPSNR (dB) measure of image reconstruction quality of the proposed joint demosaicker (center) and five existing demosaickers. Chromatic aberration correction for the latter was performed both pre-demosaicking (left) and post-demosaicking (right). These are for the Compact camera optical pipeline (top) and DSLR camera optical pipeline (bottom).

6. CONCLUSION

In this paper we studied the interaction of algorithmic Chromatic Aberration correction with the mosaicking-demosaicking step of image capture and found both standard techniques of CA correction, before and after demosaicking, to be problematic. Of the two, we found CA correction before demosaicking to be superior.

Figure 1. Original image with chromatic aberration (left) and the reconstructed image with chromatic aberration removed.

Next, we formulated a joint demosaicking and chromatic aberration correction algorithm that significantly outperforms both pre and post-demosaic CA correction. This extension allows the demosaicker of[6] to reverse any image distortion specified by a linear operator, to the extent image information is not discarded by the distortion, and thus addresses both lateral and longitudinal CA. While this formulation can also be used to correct non-chromatic aberrations, such as radial distortions, it is no better in this role than the more modular technique of post demosaic correction.

The joint demosaicking and CA correction algorithm developed in this paper is a linear operator that can be implemented as a space variant FIR filter. This algorithm can readily incorporate adaptive directional spectral models, such as that of,[6] and the underlying formulation itself can be adapted to compressive sensing techniques for even better, albeit compute intensive, image reconstruction.

REFERENCES

[1] Boult, T. and Wolberg, G., "Correcting chromatic aberrations using image warping," in [*Proc. of IEEE CVPR*], 684–687 (1992).

[2] Kaufmann, V. and Ladstädter, R., "Elimination of color fringes in digital photographs caused by lateral chromatic aberration," in [*Proceedings of the XX International Symposium CIPA*], **26**, 403–408 (2005).

[3] Mallon, J. and Whelan, P., "Calibration and removal of lateral chromatic aberration in images," *Pattern recognition letters* **28**(1), 125–135 (2007).

[4] Kang, S., "Automatic removal of chromatic aberration from a single image," in [*Proc. of IEEE CVPR*], 1–8 (2007).

[5] Chung, S., Kim, B., and Song, W., "Detecting and eliminating chromatic aberration in digital images," in [*Proc. of IEEE ICIP*], 3905–3908 (2009).

[6] Singh, T. and Singh, M., "Disregarding Spectral Overlap - a unified approach for Demosaicking, Compressive Sensing and Color Filter Array Design," in [*Proc. of IEEE ICIP*], (2011).

[7] Hel-Or, Y., "The canonical correlations of color images and their use for demosaicing," *Technical Report HPL-2003-164R1, Hewlett Packard Labs, Israel* (2004).

[8] Zhang, X. and Wandell, B., "A spatial extension of CIELAB for digital color-image reproduction," *Journal of the Society for Information Display* **5**(1), 61–63 (1997).

[9] Wang, Z., Bovik, A., Sheikh, H., and Simoncelli, E., "Image quality assessment: From error visibility to structural similarity," *IEEE Trans. on Image Processing* **13**(4), 600–612 (2004).

[10] Zhang, L. and Wu, X., "Color demosaicking via directional linear minimum mean square-error estimation," *IEEE Trans. on Image Processing* **14**(12), 2167–2178 (2005).

[11] Hirakawa, K. and Parks, T., "Adaptive homogeneity-directed demosaicing algorithm," *IEEE Trans. on Image Processing* **14**(3), 360–369 (2005).

[12] Malvar, H., He, L., and Cutler, R., "High-quality linear interpolation for demosaicing of Bayer-patterned color images," in [*Proc. of IEEE ICASSP*], **3**, 485–488 (2004).

[13] Gunturk, B. K., Member, S., Altunbasak, Y., Member, S., and Mersereau, R. M., "Color plane interpolation using alternating projections," *IEEE Trans. on Image Processing* **11**, 997–1013 (2002).

[14] Leung, B., Jeon, G., and Dubois, E., "Least-Squares Luma-Chroma Demultiplexing Algorithm for Bayer Demosaicking," *IEEE Trans. on Image Processing* **20**(7), 1885–1894 (2011).

[15] Zhang, L., Wu, A., Buades, A., and Li, X., "Color Demosaicking by Local Directional Interpolation and Non-local Adaptive Thresholding," *Journal of Electronic Imaging* **20**(2) (2011).

APPENDIX A. COLOR PLANE WARPING

As in sections 2, 3, let x_i, $x_i', i \in \{r, g, b\}$ be the aberration free and aberrated discrete image color planes respectively, and let ξ_i, ξ_i' be their continuous domain counterparts. The discrete domain image is obtained from its continuous domain counterpart by sampling with rectangular photosites. This sampling may be described as a convolution with a 2D rectangular function followed by 2D Dirac comb sampling:

$$x_i' = (\xi_i' * h_{box}).h_{sample} \tag{7}$$

where h_{box} represents the boxcar filtering effected by the rectangular pixel and is given by

$$h_{box}(u_1, u_2, w_1, w_2) \equiv Rect_2(\frac{u_1}{l_1}, \frac{u_2}{l_2}) \tag{8}$$

Here u_1 and u_2 are continuous variables spanning the sensor patch length and width and l_1 and l_2 are the photosite length and width, and

$$h_{sample}(u_1, u_2, d_1, d_2) \equiv \frac{1}{d_1 d_2} DiracComb_2(\frac{u_1}{d_1}, \frac{u_2}{d_2}) \tag{9}$$

where d_1 and d_2 are the photosite spacings.

ξ_i' may be obtained from the ideal chromatic aberration free image ξ through the warping functions $w_{1i}(u_1, u_2)$ and $w_{2i}(u_1, u_2)$ determined using existing methods for characterizing lateral CA. Formally,

$$\xi_i'(u_1, u_2) = \xi_i(w_{1i}(u_1, u_2), w_{2i}(u_1, u_2)) \tag{10}$$

Analogously to the aberrated color plane, the aberration free discrete color plane can be obtained from its continuous counterpart as follows

$$x_i = (\xi_i * h_{box}).h_{sample} \tag{11}$$

which may be formally inverted thus

$$\xi_i = x_i * h_{lpf} * h_{box}^{-1} \tag{12}$$

where h_{lpf} is a low pass interpolation filter that recovers the continuous signal, an example implementation of which is

$$h_{lpf} = \text{sinc}(\frac{2\pi u_1}{d_1}).\,\text{sinc}(\frac{2\pi u_2}{d_2}) \tag{13}$$

Equation 7 when combined with equations 10 and 12 yields

$$x_i' = (x_i * h_{lpf} * h_{box}^{-1})(w_{1i}(u_1, u_2), w_{2i}(u_1, u_2)) * h_{box} \tag{14}$$

Since convolution is associative, the lateral CA operator h_i^{lat} is given by the linear formula

$$h_i^{lat} = (h_{lpf} * h_{box}^{-1})(w_{1i}(u_1, u_2), w_{2i}(u_1, u_2)) * h_{box}, i \in \{r, g, b\} \tag{15}$$

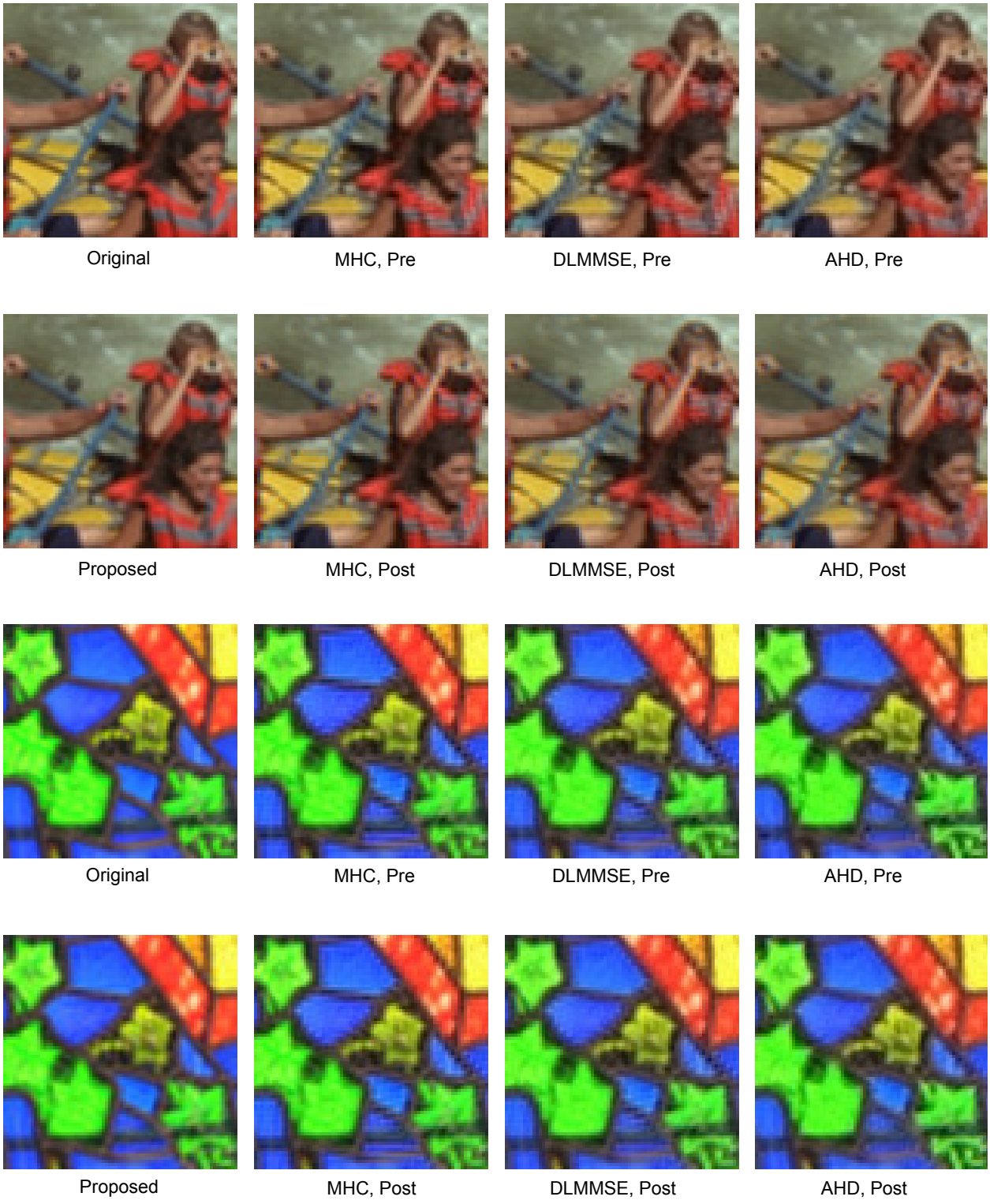

Figure 2. Original image, reconstructed image using the proposed method, MHC, DLMMSE and AHD, each of the latter three with CA correction done pre-demosaicking and post-demosaicking. The top two rows show a magnified patch of image 5 from the Kodak set and the bottom two rows show a magnified patch of image 1 from the McMaster set, both under DSLR settings.